Dieter R. Enzmann, MD • Norbert J. Pelc, ScD

Normal Flow Patterns of Intracranial and Spinal Cerebrospinal Fluid Defined with Phase-Contrast Cine MR Imaging[1]

A phase-contrast cine magnetic resonance (MR) imaging technique was used to study normal dynamics of cerebrospinal fluid (CSF) in 10 healthy volunteers and four patients with normal MR images. This pulse sequence yielded 16 quantitative flow-encoded images per cardiac cycle (peripheral gating). Flow encoding depicted craniocaudal flow as high signal intensity and caudocranial flow as low signal intensity. Sagittal and axial images of the head, cervical spine, and lumbar spine were obtained, and strategic sites were analyzed for quantitative CSF flow. The onset of CSF systole in the subarachnoid space was synchronous with the onset of systole in the carotid artery. CSF systole and diastole at the foramen of Monro and aqueduct were essentially simultaneous. The systolic and diastolic components were different in the subarachnoid space, where systole occupied approximately 40% and diastole 60% of the cardiac cycle, compared with the ventricular system, where they were equal. This difference results in systole in the intracranial and spinal subarachnoid spaces preceding that in the ventricular system; the same is true for diastole. The fourth ventricle and cisterna magna serve as mixing chambers. The high-velocity flow in the cervical spine and essentially no flow in the distal lumbar sac indicate that a portion of the capacitance necessary in this essentially closed system resides in the distal spinal canal.

Index terms: Cerebrospinal fluid, MR studies, 10.1214, 30.1214 • Cerebrospinal fluid, flow dynamics, 10.91, 30.91

Radiology 1991; 178:467–474

ALTHOUGH some fundamental features of cerebrospinal fluid (CSF) flow physiology have been known for some time, a more detailed understanding of CSF motion has been gained with the use of magnetic resonance (MR) imaging techniques (1–4). The sensitivity of MR imaging to motion was used to advantage in a study performed to characterize CSF motion in various parts of the neuraxis (5). An important feature of this early MR investigation was the confirmation of brain motion in addition to CSF motion. In this early study, the MR data were somewhat limited in time resolution and were not in an image format (5). More recent developments of pulse sequence have allowed generation of MR velocity images that yield quantitative flow information (6–9). Although initially applied to investigating the vascular system (10), the sequences have been adapted for use in studying CSF physiology.

This investigation was undertaken to characterize and quantitate normal CSF flow at key locations in the intracranial and spinal neuraxis by means of a phase-contrast cine MR pulse sequence. The main purpose of this study was to use CSF velocity profiles to define the direction of CSF flow in ventricular and subarachnoid locations throughout the cardiac cycle. This important basic information is useful for understanding altered physiology in disease states such as syringomyelia and the various forms of hydrocephalus. The cine technique is advantageous because it provides dynamic data and phase relationships not available with nongated techniques of flow imaging.

MATERIALS AND METHODS

The phase-contrast MR pulse sequence used in this study is a derivative of a cardiac cine MR sequence in which the spectrometer cycles at a constant rate (asynchronous to the cardiac cycle) with timing of the phase-encoding increments driven by the cardiac cycle trigger (8). In the modified method, two sequences that interrogate the same section but contain different flow encoding are interleaved during each cardiac cycle (9). The differential flow encoding consists of different first moments of the magnetic field gradient in a selected direction. After Fourier transformation, pixel-by-pixel phase differences are proportional to velocity in the encoded direction (6,7,10). Gradient waveforms in the other directions are unchanged. If the readout or section select directions are not being flow encoded, first-order moment nulling is used in those directions to reduce artifacts.

The sensitivity to flow is selectable and parameterized by the encoding velocity, V_{enc}, that causes a differential phase shift of 180° to be observed. Choosing smaller V_{enc} values improves precision. On the other hand, V_{enc} values should not be too small because velocities greater than V_{enc} in absolute value are aliased, have an error that is a multiple of 2 V_{enc}, and appear erroneously inside the $\pm$ V_{enc} range. This flow aliasing is readily recognized because, when it occurs, adjacent pixels have very different velocities (sharp transitions from black to white). Two velocity ranges were used with V_{enc} values of 15 cm/sec for CSF flow and 60 cm/sec for the carotid arteries. The images were obtained separately. Flow encoding was craniocaudal (section select gradient) in all subjects.

A maximum of two planes could be imaged simultaneously. In an interleaved

[1] From the Department of Diagnostic Radiology and Nuclear Medicine, Stanford University Medical Center S-072, 300 Pasteur Dr, Stanford, CA 94305. Received March 12, 1990; revision requested May 1; final revision received and accepted September 21. **Address reprint requests to** D.R.E.

Abbreviations: CSF = cerebrospinal fluid, SEM = standard error of the mean, V_{enc} = velocity of cerebrospinal fluid that causes a differential phase shift of 180°.

two-plane acquisition, the first plane is interrogated with the first flow encoding, which is followed by the second plane being interrogated with the first flow encoding, then the first plane with the second flow encoding, and finally the second plane with the second flow encoding. This set of sequences is repeated with the same phase-encoding throughout one cardiac cycle. On detection of a cardiac trigger, the phase-encoding value is incremented. The imaging time can be as short as 128 cardiac periods (256 × 128, one signal averaged), but we used 256 × 128 with two signals averaged. For a sequence time of 27 msec and single-plane acquisition, the temporal resolution is approximately 54 msec because the two flow encodings are interleaved. If two planes are interleaved as well, the temporal resolution is 108 msec. Because the two flow encodings are interleaved, the "repetition time" for any single flow experiment is twice the sequence time, or 54 msec in our case. For this reason, the single-section temporal resolution is approximately 54 msec. If two sections are interleaved as well, the repetition time (in a nuclear MR sense) is 54 msec and the temporal resolution is 108 msec.

The data acquired for each of the planes and each of the flow encodings in each cardiac cycle were separately sorted and interpolated into data sets for a selectable number of cardiac phases (8). We used 16 points in the cardiac cycle. The pulse sequence was a variant of gradient recalled acquisition in the steady state (8), in which the phase-encoding axis is rephased after the echo and a constant spoiler at the end of the sequence is used. We used a flip angle of 30°, an echo delay of 13 msec, an acquisition window of 8 msec, and a field of view of 24 cm. All studies were performed with a 1.5-T imager (Signa; GE Medical Systems, Milwaukee). Magnitude and phase reconstructions of each of the data sets were performed. The magnitude images were essentially equivalent to cine MR images obtained with conventional gradient echos and partial flip angles. The magnitude images from both flow experiments at each cardiac phase were averaged to improve the signal-to-noise ratio. For each plane and each phase of the cardiac cycle, the phase images were subtracted to produce images proportional to the flow velocity in the direction of the selected flow encoding.

Eddy current effects of the magnetic field gradient that are different in the two flow experiments can cause background phase shifts in the image. Owing to their source, these effects are primarily constant or linearly varying across the image. The presence of these effects was estimated and compensated for by means of a weighted (by magnitude squared) least-squares fit and then subtracted. The resulting images could be used to portray flow quantitatively, with zero representing no flow, positive values indicating flow in one direction, and negative values indicating motion in the other direction. If all the spins in a voxel move similarly, this technique is quantitative without needing calibration, as has been shown by Spritzer et al for the ungated version of this technique (10).

The conditions required for quantitative data are met if flow is through the section. Images in which each pixel in the phase-difference image is multiplied by the corresponding pixel in the magnitude image for each cardiac frame can also be generated; they are more aesthetic because flowing fluids are highlighted and the background noise level is suppressed because of its relative signal magnitude. For the resulting images, lack of flow is seen as an intermediate shade of gray, craniocaudal flow is depicted as high signal intensity, and caudocranial flow is shown as low signal intensity.

Fourteen persons were studied: 10 healthy volunteers (six women and four men aged 23–42 years) and four patients with normal MR images (two women and two men aged 36–68 years). They were segregated into three different groups. The first group, consisting of five healthy volunteers, underwent an extensive protocol in which axial and sagittal phase-contrast images of the head and spine were obtained. Intracranial axial sections were 5 mm thick, and spinal axial sections were 10 mm thick; all sagittal sections were 10 mm thick. In the brain, the foramen of Monro, aqueduct, and fourth ventricle were imaged axially. In the spine, axial images were obtained at the C1-2 and C6-7 levels. Sagittal imaging was performed at a midline intracranial location to visualize the fourth ventricle and cisterna magna. The quadrigeminal cistern was visualized at the aqueduct level. The sagittal image of the cervical spine showed both the anterior and posterior subarachnoid space. A sagittal image of the lumbar region extending up to T-9 was also obtained. The axial images were used to measure the velocity profiles throughout the cardiac cycle at each of these anatomic locations. The axial images of the cervical spine also allowed determination of flow in the epidural venous plexus.

A second group of four patients underwent a more limited examination that included only the upper cervical spine. However, two types of images were obtained at the same axial location, one for determining CSF flow (V_{enc} = 15 cm/sec) and a second for determining blood flow in the carotid arteries and jugular veins (V_{enc} = 60 cm/sec). Two images (V_{enc} = 15 and V_{enc} = 60 cm/sec) were required because of the vastly different velocities of CSF and arterial blood. From these data, CSF velocity profiles for the cervical subarachnoid space, the carotid artery, the jugular vein, and the epidural venous plexus were generated. This allowed correlation of the flow patterns of two systems, one of which is presumed to drive the other.

A third group of five patients underwent axial imaging of the foramen of Monro, aqueduct, and the C1-2 level. At the last level, two images were obtained with two flow-encoding ranges to measure CSF flow and vascular blood flow (carotid and jugular).

Velocity measurements were derived from phase-contrast MR images. Round or elliptic regions of interest (0.04–0.25 cm^2) were defined on axial images obtained at the foramen of Monro, aqueduct, fourth ventricle, cisterna magna, and medial and lateral cervical subarachnoid space and in the internal carotid artery, internal jugular vein, epidural venous plexus within neural foramina in the cervical spine, and the subarachnoid space anterior to the conus. The smallest regions of interest were limited to small aqueducts and the epidural venous plexus. The direction of flow was through the plane and parallel to the flow-encoding axis at all of these anatomic sites except the aqueduct. The aqueduct measurement was made at its junction with the fourth ventricle to minimize the angle of the flow with the flow-encoding axis and to minimize the partial volume effect. The small residual angle with the section resulted in some underestimation of velocities; the shape of the flow curve, however, was unaffected.

To correct for the possibility of residual systematic errors caused by imperfect suppression of eddy current, a background baseline value representing the apparent velocity in a region of no flow was recorded for each series of images and was subtracted from the apparent velocities in the region of interest. The flow, expressed in millimeters per second, was the difference between the apparent velocity of the CSF or vascular space and the background at 16 points in the cardiac cycle. Pulsation amplitude for the region of interest could be calculated from these data by summing incremental motion in each frame by means of the actual heart rate. This allowed determination of maximum cranial and caudal displacement of CSF, the difference between which represented the pulsation amplitude.

To normalize findings among patients with different heart rates, the delay with respect to the gating trigger of each frame was converted to a percentage location within the cardiac cycle. In this way, patient data could be combined and compared. This normalization was possible for this group of patients with normal MR images because their heart rates were in a relatively narrow range (67–82 beats per minute). The cardiac cycle in this study was determined with a peripheral gating trigger (photoplethysmograph on a finger). This device was chosen because it was simple and fast to use and provided a trigger more reliable than an electrocardiographic signal in our system at the time of this study.

Peak velocity in systole and diastole in the cardiac cycle and the temporal location of peak systolic and peak diastolic velocity as a percentage of the cardiac cycle were measured. Maximum excursion values for systole and diastole were calcu-

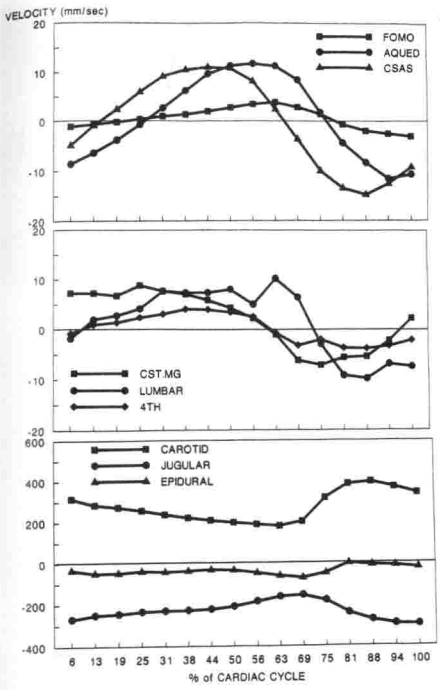

Figure 1. Graphs representing velocity (millimeters per second) versus relative location in the cardiac cycle. Curves are for the following sites: foramen of Monro (*FOMO*), aqueduct (*AQUED*), cervical subarachnoid space (*CSAS*), cisterna magna (*CST.MG*), lumbar spine, fourth ventricle (*4TH*), carotid artery, jugular vein, and cervical epidural veins at the C-1 to C-2 level. Negative numbers indicate craniocaudal motion, while positive numbers show caudocranial motion. Bottom graph has a wider velocity scale for the blood velocity curves. Sixteen data points are defined as a percentage of the cardiac cycle, allowing patients with different heart rates to be compared and averaged. These curves represent the mean velocities for all patients who underwent cine MR imaging at the above locations. (**Top**) Where curves cross the zero baseline is the point at which reversal of flow occurs. Note that while the cervical subarachnoid space and aqueduct had similar velocity profiles, they were slightly out of phase, with systolic (craniocaudal) CSF motion occurring earlier in the cervical subarachnoid space than in the aqueduct. Flow reversal occurred at 66% through the cardiac cycle in the cervical subarachnoid space and at 75% through the cardiac cycle in the aqueduct and the foramen of Monro. Similarly, reversal of CSF in diastole occurs earlier in the cervical subarachnoid space (13%) than in the aqueduct and foramen of Monro (25%). Diastole is of longer duration than systole, approximately in a 60:40 proportion. Mean velocities in the aqueduct were similar to those recorded at the C1-2 anterior subarachnoid space. (**Middle**) Cisterna magna and fourth ventricle have a similar velocity pattern. Flow reversal (diastole to systole) in these locations is simultaneous with that in the cervical subarachnoid space (63%). Velocities are lower than in the aqueduct or cervical subarachnoid space. The slight upward deviation of the fourth ventricular curve at 75% is indicative of mixing of CSF from upward flow through the valecula. The CSF velocity profile in the lumbar spine at the level of the conus is somewhat more irregular but still shows systolic and diastolic components. (**Bottom**) Carotid systole is virtually simultaneous with CSF systole in the cervical subarachnoid space. This is best seen in the graph of an individual patient (Fig 2). The onset of carotid systole is simultaneous with increased velocity of blood in the internal jugular vein. There is no reversal of flow in either the internal carotid artery or jugular vein. As is evident from the curves, other than the onset of CSF systole there is no consistent relationship between blood velocity and CSF flow.

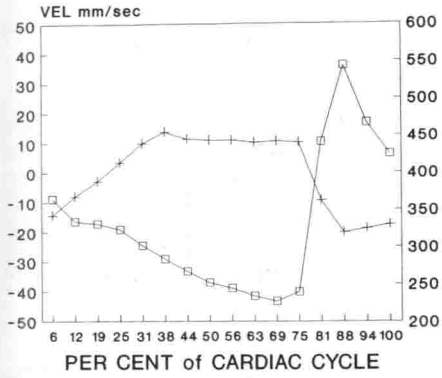

Figure 2. Velocity (*VEL*) profile within the cervical subarachnoid space at C1-2 and in the carotid artery in one patient. The CSF velocity scale is shown on the left vertical axis, while the blood velocity scale is shown on the right. The 16 data points on the horizontal axis represent percentages of the cardiac cycle. Typical findings, as illustrated here, include carotid systole (□) simultaneous with cervical subarachnoid space systole (+).

lated to determine pulsation amplitude. The graphs in Figure 1 represent the mean values of all patients and volunteers. In these plots the horizontal axis represents temporal location as a percentage of the cardiac cycle and the vertical axis represents the velocity of CSF or blood in millimeters per second. The standard error of the mean (SEM) was calculated for peak systolic and diastolic velocities and for the times of peak systolic and peak diastolic velocity at each anatomic site. As is pointed out, partial volume effects at the appropriate anatomic site could cause an underestimation of peak velocity at sites such as the foramen of Monro, where an image of a 10-mm section included CSF flow moving slower than the jet of CSF in the actual foramen. This same effect probably occurred on images of small aqueducts in which brain parenchyma may have been subject to partial volume effects. Small regions of interest and proper section positioning were used to minimize this partial volume effect. In the cervical subarachnoid space partial volume effects were minimal even with 10-mm sections.

RESULTS

Foramen of Monro

Small jets of flow were identified with this pulse sequence bilaterally in the lateral ventricles just above the foramen of Monro (Fig 3a–3h). Systolic flow was craniocaudal with peak velocity occurring at 100% (SEM = 4.3%) through the cardiac cycle as defined with peripheral gating (Fig 1, top). Maximum diastolic velocity (ie, caudocranial flow) occurred at 63% (SEM = 4.7%) through the cardiac cycle. CSF systole and diastole were nearly equivalent in duration. Mean peak diastolic velocity (5.5 [SEM = 1] mm/sec) was nearly equivalent to mean peak systolic velocity (4.1 [SEM = .5] mm/sec). This small difference between systolic and diastolic mean peak velocities was not unexpected given the potential for partial volume error in the foramen of Monro because of the variable size of the "jet" effect at different points in the cardiac cycle. The calculated pulsation amplitudes in this region were approximately 1.5 mm.

Ventricles

Velocity changes in the frontal horns were minimal and did not have a clear oscillatory pattern. In most patients no significant motion was detected, but in five patients a short period of craniocaudal displacement was seen during systole. The change was uniform throughout the frontal horns; there were no flow channels except at the foramen of Monro. Sagittal views showed downward displacement of the genu of the corpus callosum early in systole.

Aqueduct

The velocity profile of CSF in the aqueduct was similar to that of CSF in the foramen of Monro although velocities were greater (Fig 1, top; Fig 3i–3p). CSF systole and diastole were essentially equivalent in duration. Peak systolic flow (craniocaudal flow) occurred at 94% (SEM = 2.3%) through the cardiac cycle, whereas peak diastolic flow occurred at 56% (SEM = 3.3%) through the cardiac cycle. Flow was reversed simultaneously in the foramen of Monro and aqueduct at 75% through the cycle. Mean peak velocities were nearly

equivalent during the systolic and diastolic phases: 11.6 (SEM = 3.4) and 11.8 (SEM = 5.0) mm/sec, respectively. Pulsation amplitudes were approximately 5 mm. Both the peak velocities and pulsation amplitudes are slight underestimates because of the small angle between the direction of flow in the aqueduct and the direction of velocity encoding.

Fourth Ventricle

The fourth ventricle represented a mixing chamber for CSF exiting the ventricular system and CSF flowing in from the cisterna magna (Fig 4). CSF could be visualized moving in craniocaudal and caudocranial directions simultaneously within the fourth ventricle. Nevertheless, sys-

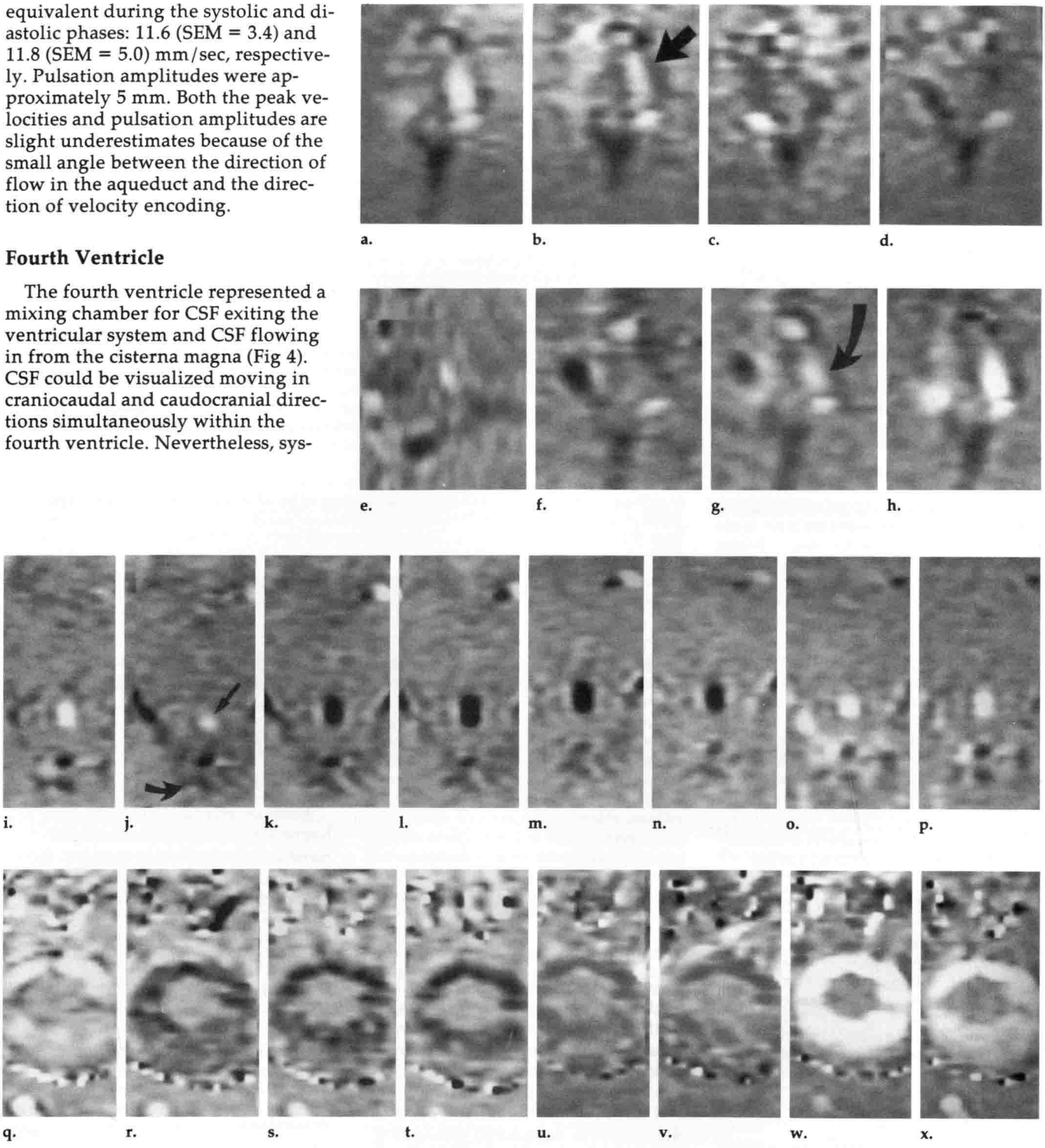

Figure 3. Velocity-encoded images at three sites: foramen of Monro, aqueduct, and cervical subarachnoid space in the same patient. Onset of systole for these three sites is between images **f** and **g**, **n** and **o**, and **v** and **w**, respectively. **(a–h)** Series of eight velocity-encoded images of an axial section through the foramen of Monro. High signal intensity represents craniocaudal flow (CSF systole); low signal intensity represents caudocranial flow (CSF diastole). Alternate images of the 16 total images are illustrated. Onset of CSF systole, simultaneous with that in the aqueduct, is indicated by high signal intensity (**g**, arrow). In transition from systole to diastole, high signal intensity is seen in the foramen (**b**, arrow) and in the aqueduct (**j**, straight arrow), while cervical subarachnoid space (**r**) already has low signal intensity, indicating reversal of flow (ie, CSF diastole). CSF diastole occurs earlier in the subarachnoid space than in the ventricular system. **(i–p)** Series of eight velocity-encoded images of an axial section through the lower aqueduct. Flow encoding is the same as at other sites. At level of the aqueduct, systole and diastole each represent approximately 50% of the cardiac cycle. Onset of systole appears simultaneously with that in the subarachnoid space in this series of images (**o** and **w**). Image not depicted between **v** and **w** showed onset of cervical subarachnoid space systole while the aqueduct was still in CSF diastole. This delay in aqueduct systole compared with the cervical subarachnoid space is again seen in transition from systole to diastole. While the aqueduct is in systole (**j**, straight arrow), CSF in cervical subarachnoid space is already in diastole (**r**). Similar difference exists between aqueductal flow and quadrigeminal cistern flow (**j**, curved arrow). **(q–x)** Series of eight axial velocity-encoded MR images (alternate image of 16 total images) of the cervical subarachnoid space at the C1-2 level. Onset of CSF systole actually was in image between **f** and **g** not depicted here. End of systole and onset of diastole is seen in the transition from **q** to **r**. At this cervical level CSF systole is approximately 40% of the cardiac cycle, whereas diastole represents approximately 60% of the cardiac cycle.

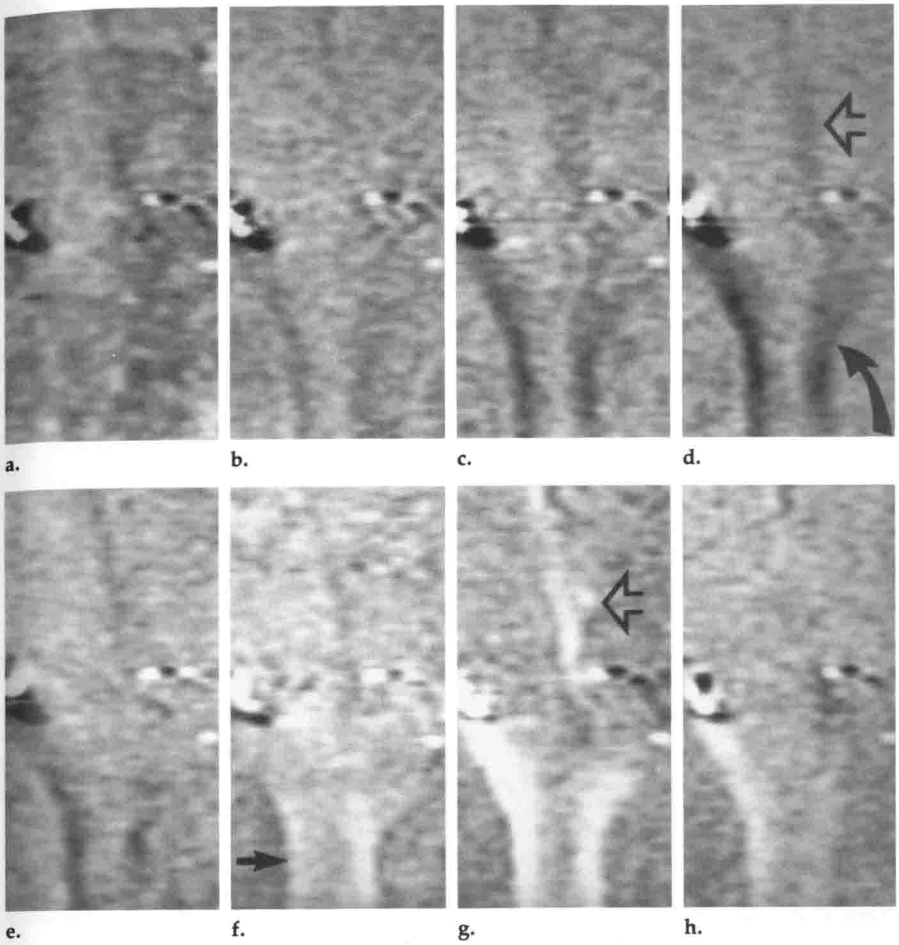

Figure 4. **(a–h)** Sagittal velocity-encoded images of the craniocervical junction. (Craniocaudal flow is white, caudocranial flow is black.) Onset of systole is seen in **f** (arrow), which shows high signal intensity in the subarachnoid space. Diastolic flow is seen in **d** in the fourth ventricle (open arrow) and the cisterna magna (curved arrow). One can see both high and low signal intensity in the fourth ventricle, indicating bidirectional CSF flow, that is, mixing of CSF (**g**, arrow).

tolic and diastolic phases were evident (Fig 1, middle). The velocity profile was generally similar to that of the cervical subarachnoid space (Fig 1, top). At 75% through the cycle a consistent short reversal of flow was detected in the fourth ventricle that coincided with inflow of CSF caused by the earlier flow reversal in the cervical subarachnoid space and cisterna magna (Fig 1, middle). Because the sagittal images were acquired to better demonstrate mixing, measured phase shifts may underestimate true velocities because of partial volume error. However, the measured temporal relationships are expected to be accurate.

Cisterna Magna

The cisterna magna represented the other major site of mixing CSF of the ventricular system with that of the subarachnoid space. Systolic and diastolic phases could be identified but were less well defined than those of the other areas studied (Fig 1, middle). Craniocaudal and caudocranial flow could often be detected simultaneously. Because of the anatomy and mixing characteristics, pulsation amplitude had little meaning in this location. The larger size of the cisterna magna compared with the fourth ventricle makes it less susceptible to partial volume error in determining the velocity magnitude.

Cervical Spine

The CSF pulsation dynamics in this location showed well-defined systolic and diastolic components (Figs 3q–3x, 5). Peak velocity (craniocaudal flow) during CSF systole occurred at 88% (SEM = 2.7%) through the cardiac cycle, and peak diastolic velocity occurred at 44% (SEM = 2%) through the cardiac cycle. Peak systolic velocity of CSF was simultaneous with peak systolic velocity of the carotid artery (Fig 2); both just preceded the peripheral trigger. It is noteworthy that peak systolic velocity in the cervical spine subarachnoid space preceded peak systolic velocity in the foramen of Monro and aqueduct by 10%–14% of the cardiac cycle. This difference was consistent among patients. Mean peak systolic velocity in the anterolateral recess was 14.8 (SEM = 1.9) mm/sec, while peak diastolic velocity was 11.1 (SEM = 1.0) mm/sec. These figures represent averages in the areas of highest flow in the subarachnoid space. The velocities in the subarachnoid space were heterogeneous because of the various compartments formed by dorsal and ventral roots, the dentate ligament, and dorsal arachnoid septations. The velocities in the anterior subarachnoid space were not significantly different from those of the anterolateral recesses. Velocities dorsal to the cervical cord were lower and more variable; in some patients no flow was detected dorsal to the cord except during peak systole and diastole (Figs 3q–3x, 5i–5p). The timing of the velocity changes, however, was uniform in these flow compartments. Therefore, the size of the region of interest does not affect the measurement of timing relationships.

The calculated pulsation amplitude in the cervical spine varied with location in the anterior subarachnoid space. In the midline at the C1-2 level the pulsation amplitude was in the range of 4–5 mm, whereas in the anterolateral recesses the pulsation amplitude was in the range of 7–9 mm. The pulsation amplitude at the level of C6-7 was more uniform in the narrower anterior subarachnoid space and was about 9 mm (Fig 5). In most patients, CSF motion in the subarachnoid space anterior and dorsal to the spinal cord was in synchrony. In two patients, craniocaudal flow in the anterior cervical subarachnoid space in late systole was accompanied by caudocranial flow in the posterior subarachnoid space; that is, reversal of flow occurred earlier posterior to the cord.

Lumbar Spine

Measurements of the thoracolumbar junction anterior to the conus were made. That location was the only area where consistent flow was detectable in the lower spine and where systolic and diastolic components were definable. Maximum peak systolic velocity occurred at 88% (SEM = 3%) through the cardiac cycle, while maximum diastolic velocity occurred at 63% (SEM = 7.5%)

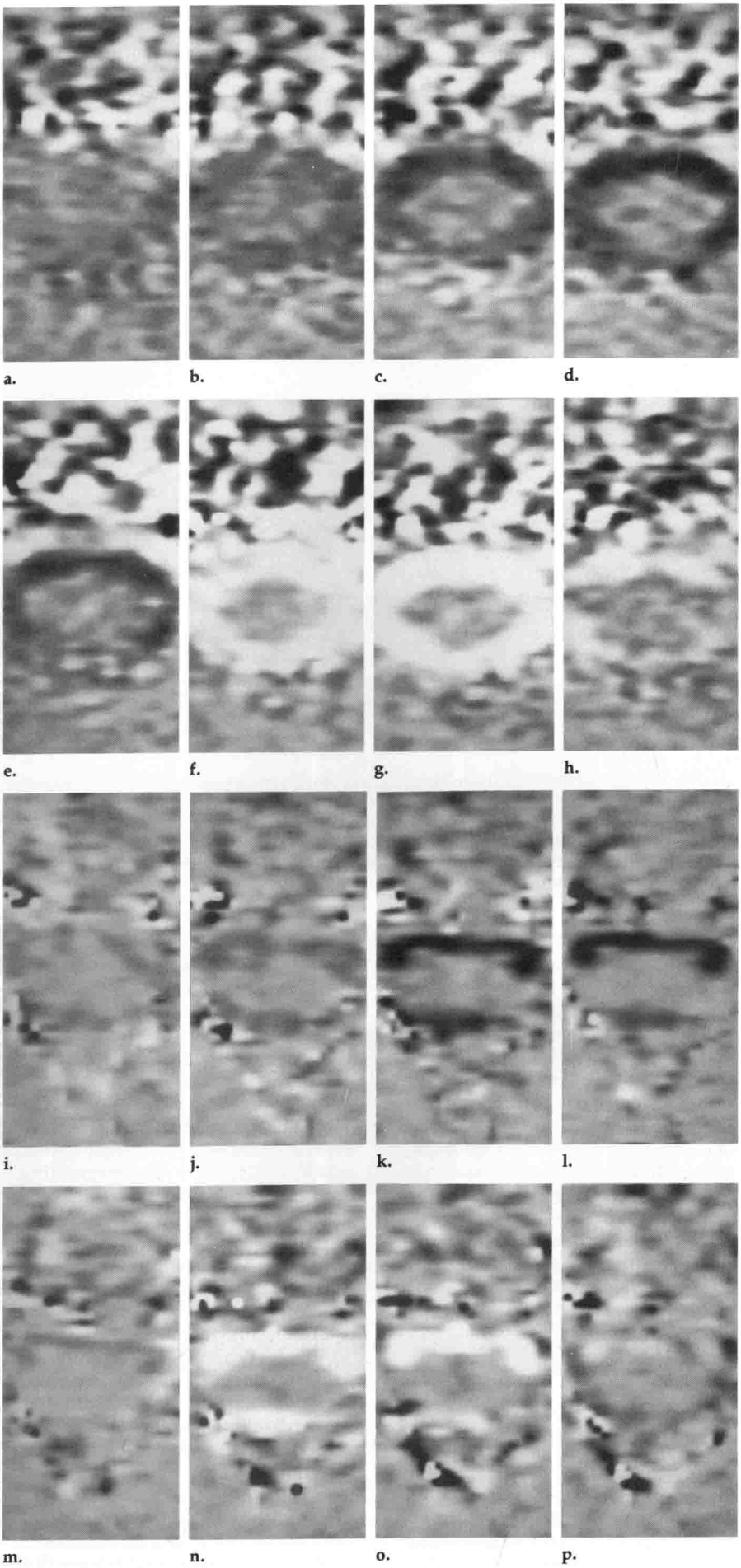

Figure 5. **(a-h)** Axial velocity-encoded images of cervical subarachnoid space show relatively symmetric flow around the cord in both the anterior and posterior subarachnoid space. Onset of systole is seen in **f**, while onset of diastole is seen in **a.** **(i-p)** In same patient a simultaneous acquisition shows CSF flow pattern at the C6-7 level. Note the different distribution of CSF flow, with most flow occurring in the anterior subarachnoid space, especially the anterolateral recesses. Velocity profile during the cardiac cycle was identical to that seen at the C1-2 level except that peak velocities were higher at the C6-7 level. Some bidirectional flow is seen at the C6-7 level in the anterior subarachnoid space **(p)**.

through the cycle (Fig 1, middle). The mean systolic and diastolic flow velocities just anterior to the conus were 9.8 (SEM = 2) mm/sec and 10.3 (SEM = 4.2) mm/sec, respectively. Pulsation amplitudes were about 4 mm. No flow was identified in the distal lumbar sac with the velocity range used in these measurements.

Electrocardiographic versus Peripheral Gating

Because previous studies involved electrocardiographic gating and this study involved peripheral gating, velocity profiles for the aqueduct and cervical subarachoid space observed with these two gating methods were compared in two patients. The profiles were the same, with peak systolic velocities being displaced to the left, that is, occurring 65%–70% earlier in the cardiac cycle, when defined with electrocardiography than when defined with peripheral gating. The cardiac cycle defined with peripheral gating contains the diastolic portion of the period preceding the beat. Nevertheless, as long as the cardiac period is relatively consistent, the relationship between systole and diastole at the different sites is the same with either peripheral gating or electrocardiographic gating.

Internal Carotid Artery

Peak systolic velocity occurred at 88% (SEM = 2%) through the cardiac cycle, which means peak flow occurred just before the peripheral pulse trigger. There was no reversal of flow. Minimum velocity occurred at 63% through the cycle. Peak velocity in the carotid artery was virtually simultaneous with the peak craniocaudal CSF velocity in the cervical subarachnoid space. The mean peak

velocity in the internal carotid artery at the C-1 to C-2 level was 430 (SEM = 27) mm/sec.

Internal Jugular Vein

Peak systolic velocity in the jugular vein occurred at 98% (SEM = 3.5%) through the cardiac cycle, that is, later than peak velocity in the internal carotid artery and peak CSF flow in the cervical subarachnoid space. The minimum velocity occurred at 70% (SEM = 3.2%) through the cardiac cycle. The mean maximum systolic velocity was 310 (SEM = 41) mm/sec. In this group, the jugular veins were relatively symmetric.

Epidural Veins

The flow characteristics in the spinal epidural veins varied among patients and also among levels within a patient. At the C1-2 level, flow along the flow-encoding axis could oscillate or be unidirectional through the entire cardiac cycle. Blood flow in the C1-2 foraminal venous sinuses on the right and left side of the spinal canal could oscillate in unison or alternately. The epidural sinuses in the neural foramina at the C6-7 level showed more consistent findings from side to side, but there was still variability within the cardiac cycle. Thus the flow characteristics in the cervical epidural venous plexus did not show a consistent phase relationship with CSF flow in the cervical subarachnoid space.

DISCUSSION

Although the specific pulse sequences and the gating techniques used to define the cardiac cycle differ, the phase-contrast cine MR technique employed in this investigation confirms and extends previous observations of the CSF circulation (5). The patterns of CSF oscillation through the foramen of Monro and aqueduct confirm that the lateral ventricles, rather than a third ventricular "CSF pump," play the major role in normal CSF flow within the ventricular system. CSF pulsations at the foramen of Monro and aqueduct are in synchrony. Flow through the foramina of Monro appeared as small jets of flow, while the remainder of the lateral ventricles showed no focal velocity changes.

CSF systole and diastole within the ventricular system are slightly out of phase with CSF systole and diastole in the subarachnoid space, the ventricular flow being slightly delayed compared with that of the subarachnoid space. This finding was observed in each subject and is not the result of data averaging. This difference in flow results in the fourth ventricle and cisterna magna acting as mixing chambers. In most CSF spaces, fluid motion is uniform in one direction, but in the fourth ventricle and in the cisterna magna, motion is more complex, showing craniocaudal and caudocranial flow simultaneously in the systolic and diastolic time segments in the cardiac cycle.

CSF systole as indicated by onset and peak craniocaudal flow is simultaneous in the suprasellar, prepontine, and quadrigeminal cisterns and the cervical spine subarachnoid space. This pattern of flow shows that subarachnoid CSF moves unidirectionally and in synchrony during systole. The pattern is similar but slightly delayed in the upper lumbar spine. During systole, some of the smaller veins in the quadrigeminal cistern collapse. The epidural veins in the cervical spine showed no direct or consistent relationship to CSF systole. Flow in the spinal epidural venous plexus was variable; it could be oscillatory or unidirectional (often craniocaudal) throughout the cardiac cycle.

With the velocity profiles measured in strategic locations and the qualitative assessment of the flow in the quadrigeminal and suprasellar cisterns, one can piece together the hydrodynamics of normal CSF flow. In normal persons, this study showed that CSF systole and diastole are slightly out of phase between the ventricular system and the subarachnoid space. In the ventricular system the oscillatory flow is such that systole and diastole each occupy approximately 50% of the cardiac cycle and, not surprising, the velocities are nearly the same in both directions. This is true for the foramen of Monro and aqueduct. Since the brain is incompressible, this nearly equivalent oscillatory flow in systole and diastole is to be expected in a closed system with a low CSF production rate. During a single cardiac cycle, no significant inflow or outflow of CSF occurs in this essentially closed system.

The timing parameters in this study are expressed as percentages of the cardiac cycle. Since changes in heart rate have a greater effect on diastole than on systole, an error could be introduced, in principle, by this averaging technique. In this study, however, the heart rates were clustered in a narrow range, and combining the data in this way was justified. Further, this averaging phenomenon is inherent in any cine acquisition if the heart rate changes during the study. Previous experience with the design of the cine sequence indicated that this linear temporal model of cine data is reasonable within the range of heart rates in this study (8).

To allow for CSF oscillation there needs to be capacitance in the system. A portion of this capacitance appears to be in the lumbar sac and is associated with the asymmetry in CSF systole and diastole in the spinal subarachnoid space. That some capacitance exists intracranially is known because veins were seen to be compressed in the quadrigeminal cistern during CSF systole. A major site of capacitance must also be the distal lumbar sac because high-flow CSF can be detected from the cervical spine to the level of the conus. Below this level, little if any flow is detected. Systole is shorter than diastole, and because net flow is not significant, peak velocities are higher in systole than in diastole. This profile of systole and diastole in the spinal subarachnoid space is maintained in the subarachnoid space up to the base of the brain, that is, the quadrigeminal cistern and suprasellar cistern. The fourth ventricle and cisterna magna provide the mixing sites for the different ventricular and subarachnoid oscillatory patterns.

Since there is no significant net CSF flow within the central nervous system during a cardiac cycle, one can use compartmental analysis to analyze CSF flow (11). The assumption is that since the brain is not compressible and there is no net CSF flow in or out, capacitance must be provided by a comparable volume of fluid (blood) or tissue displacement. Capacitance in the CSF space implies reserve volume produced by displacement or compression, or both, of tissue, most likely epidural veins and fat. During systole, carotid inflow velocity profiles show earlier inflow compared with jugular venous outflow. For a brief period, therefore, there is a net inflow of blood into the brain, causing it to expand in volume. Since there are no significant compressible structures in the intracranial space except venous structures, this expansion of brain blood volume causes caudal displacement of a comparable volume of CSF from the ventricular system and intracranial subarachnoid space into

the spinal subarachnoid space. Brain expansion decreases CSF volume within both the ventricular system and the surrounding subarachnoid space.

The configuration of the brain is such that its expansion is not uniform in all directions but in fact is directed downward centrally. A study by Feinberg and Mark (5) demonstrated such caudal motion early in systole in the central portion of the brain at the level of the corpus callosum and even greater movement at the level of the brain stem. This brain motion would also have the effect of causing CSF flow over the convexities toward the sagittal sinus because this space could increase with the central downward motion of the brain. Although this study did not involve measurement of CSF flow in this anatomic region, CSF flow toward the arachnoid villi within the venous sinus is well known from radionuclide studies. This downward displacement of the brain is of short duration, with the brain returning to its resting position 200 msec after the R wave (5). Because of transient net inflow of blood into the system, volume is increased, thus requiring the capacitance in the lumbar dural sac. Minimal CSF flow is detected in the lumbar dural neural sac, indicating that this is the site of capacitance in the system.

The slight asymmetry in the velocity profile between arterial and venous blood also allows for outflow of this transient increase in cerebral blood volume. This decrease in volume follows the return of the downward displacement of the brain. The combination of decrease in brain volume with more venous outflow and the recoil of CSF accumulating in the lumbar sac causes reversal of CSF flow (ie, CSF diastole). Reversal of CSF flow occurs in the subarachnoid space before it occurs in the ventricular system (ie, aqueduct). This could be explained by the intracranial subarachnoid space increasing in volume as the brain returns to its normal position before ventricular volume is increased as a result of decreased cerebral blood volume. The asymmetry in diastolic flow, therefore, is related to an earlier increase in volume of the intracranial subarachnoid space compared with the increase in ventricular volume. Movement of the brain itself appears to be responsible for this asymmetry.

The phase-contrast cine MR pulse sequence provides an important window for investigating CSF flow dynamics. Not only is quantitative velocity information available, but the image format provides a visual display of the velocity distributions. The visual display makes the mixing role of the fourth ventricle and cisterna magna more evident. This method has been valuable in investigating normal CSF dynamics. It should prove equally valuable in investigating disease processes in which abnormal CSF dynamics are suspected, for example, various forms of hydrocephalus and syringomyelia (12). ■

References

1. Edelman RR, Wedeen VJ, Davis KR, et al. Multiphasic MR imaging: a new method for direct imaging of pulsatile CSF flow. Radiology 1986; 161:779–783.
2. Citrin CM, Sherman JL, Gangarosa RE, Scanlon D. Physiology of the CSF flow-void sign: modification by cardiac gating. AJNR 1987; 7:1021–1024.
3. Szeverenyi NM, Kieffer SA, Cacayorin ED. Correction of CSF motion artifact on MR images of the brain and spine by pulse sequence modification: clinical evaluation. AJNR 1988; 9:1069–1074.
4. Malko JA, Hoffman JC, McClees EC, Davis PC, Braun IF. A phantom study of intracranial CSF signal loss due to pulsatile motion. AJNR 1988; 9:83–89.
5. Feinberg DA, Mark AS. Human brain motion and cerebrospinal fluid circulation demonstrated with MR velocity imaging. Radiology 1987; 163:793–799.
6. Firmin DN, Nayler GL, Klipstein RH, Underwood SR, Rees RS, Longmore DB. In vivo validation of MR velocity imaging. J Comput Assist Tomogr 1987; 11:751–756.
7. Nayler GL, Firmin DN, Longmore DB. Blood flow imaging by cine magnetic resonance. J Comput Assist Tomogr 1986; 10:715–722.
8. Glover GH, Pelc NJ. A rapid cine MRI technique. In: Kressel HY, ed. Magnetic resonance annual 1988. New York: Raven, 1988.
9. Pelc NJ, Shimakawa A, Glover G. Phase contrast cine MRI (abstr). In: Book of abstracts: Society of Magnetic Resonance in Medicine 1989. Berkeley, Calif: Society of Magnetic Resonance in Medicine, 1989; 101.
10. Spritzer CE, Pelc NJ, Lee JN, Evans AJ, Sostman HD, Riederer SJ. Rapid MR imaging of blood flow with a phase-sensitive, limited-flip-angle, gradient recalled pulse sequence: preliminary experience. Radiology 1990; 176:255–262.
11. Pappenheimer JR, Heisey SR, Jordan EF, Downer ID. Perfusion of the cerebral ventricular system in unanesthetized goats. Am J Physiol 1962; 203:763–774.
12. Enzmann DR, Pelc NJ. CSF dynamics in normal and syringomyelia patients using phase contrast cine MR (abstr). In: Book of abstracts: Society of Magnetic Resonance in Medicine 1989. Berkeley, Calif: Society of Magnetic Resonance in Medicine, 1989; 11.